Biexciton on a one-dimensional lattice

Kunio Ishida* and Hideo Aoki
Department of Physics, University of Tokyo, Hongo, Tokyo 113, Japan

Tetsuo Ogawa
Department of Applied Physics, Osaka City University, Sugimoto, Sumiyoshi-ku, Osaka 558, Japan
(Received 18 November 1994; revised manuscript received 9 May 1995)

The biexciton (excitonic molecule) is theoretically studied in a one-dimensional (1D) tight-binding model having both long-range Coulomb interactions and on-site interactions. We solve the four-fermion problem by the numerical diagonalization method for finite systems. The effect of particle correlation over the lattice-constant length scale is shown to be essential, which makes both of the conventional variational or Heitler-London approximations and the continuum models inadequate. In the phase diagram for the biexciton state, a crossover in the response to an increase in the long-range interaction is found to emerge, and occurs concomitantly with the Frenkel-Wannier crossover for single excitons. The dependence of the biexciton binding energy on the electron-hole mass ratio is also found for varying strength of the Coulomb interaction, where the behavior drastically differs from those in 2D or 3D continuum models. Two-photon absorption spectra are also obtained.

I. INTRODUCTION

The biexciton (or excitonic molecule), a bound state of two electrons and two holes, provides an interesting many-body problem, since a biexciton may be thought of as a "positronium molecule" or a hydrogen molecule with variable electron and hole masses realized in semiconductors. The analogy with the positronium molecule for two Wannier excitons has resulted in a number of studies to clarify its nature.[1–3]

Conventionally, however, a biexciton is regarded as a bound state of two bosons (Wannier excitons), but this picture is too crude for an obvious reason: When two excitons are bound into a biexciton, we are faced with a four-fermion problem, with the correlation effect on the length scale of the lattice constant, and a bosonic picture of the biexciton where the fermion degrees of freedom are ignored cannot capture the binding mechanism. We have to instead look into the way in which two electrons and two holes are reshuffled. This should be important especially in evaluating optical properties, since they are determined by the dipole matrix elements between biexciton states and single-exciton states, which are in turn sensitive to the wave function. As we shall see, the deformation of the biexciton wave function from a superposition of two excitons does indeed enhance these matrix elements. Thus, it is imperative to treat the biexciton as a composite of four fermions. To the best of our knowledge, there has been no theoretical study of the biexciton from this viewpoint, although there exist some studies of the biexciton in terms of the "effective exciton-exciton interaction"[4] as we shall mention later.

Four-fermion approach also enables us to separately examine the electron-electron (or hole-hole) repulsion and the electron-hole attraction. The repulsion and attraction are different in magnitude, in general, so that it is necessary to study the formation of a biexciton as a function of their ratio.

Another strong motivation for the present study is the importance of working with *lattice* models. In a previous paper on a single-exciton problem,[5] we have shown that the exciton should be modeled on a discrete lattice, for which we can incorporate the intra-atomic interactions on top of the long-range Coulomb interactions, while continuum models have to make cutoff procedures. This is particularly important in one-dimensional systems, since the lower the dimensionality, the more the exciton wave function becomes compact and the behavior of electrons and holes on the atomic length scale becomes essential.[6]

From the single-exciton study on a lattice, a unified picture for the crossover between the strong-coupling (Frenkel) and weak-coupling (Wannier) regimes has indeed emerged. Namely, when we increase the strength of the long-range interaction relative to the intra-atomic one, a Frenkel exciton expands while a Wannier exciton shrinks. It becomes an intriguing problem to ask how this Frenkel-Wannier crossover manifests itself in biexcitons. We shall show that the crossover does appear in biexcitons in that a long-range interaction *prevents* the formation of a biexciton in the Wannier regime, whereas the long-range part *helps* its formation in the Frenkel regime. Further, the exciton transfer processes via electromagnetic dipole-dipole interaction are tractable only in lattice models, which provides another necessity to adopt lattice models.

In this paper, we focus on the one-dimensional (1D) problem. The reason is twofold. First, there is a class of 1D semiconductors, e.g., σ-conjugated semiconducting polymers such as polysilane, where 1D excitons coupled weakly to phonons are realized as opposed to the strong electron-lattice coupling as in polyacetylene. Quantum wires in semiconductor structures are also interesting. We must note, however, that they can only be regarded as 1D in terms of the excitonic properties when the width

0163-1829/95/52(12)/8980(12)/$06.00

of the wire is made smaller than the size (effective Bohr radius) of an exciton ($\sim$ 100 Å for GaAs).[7,8]

Second, an exciton is more tightly bound in 1D (Refs. 5 and 7) than in higher dimensions, so that the strong correlation effect in the composite four-fermion problem will become more pronounced. We shall confirm this by comparing the 1D result with those in higher dimensions.

Thus, the aim of this paper is to present a unified picture of the biexciton on a 1D lattice that encompasses both the Frenkel and Wannier limits. For this purpose, we employ a tight-binding lattice model with long-range and on-site interactions, which is solved by a numerical diagonalization for finite systems.

In doing so, we also look into the validity of conventional continuum models and the applicability of the Heitler-London and/or variational approximations around the Frenkel-Wannier crossover. One notable work is by Bányai *et al.*,[8] who studied the biexciton in a 1D continuum model using the effective-mass approximation and the Heitler-London scheme in terms of an "effective hole-hole potential," to obtain the binding energy as a function of the ratio of the electron and hole masses. Several approximations are involved there, however, and we reexamine the problem quantitatively with a numerical diagonalization method.

This paper is organized as follows. Section II describes the 1D lattice model. Stability of a biexciton is studied in Sec. III in terms of the biexciton binding energy and the hole-hole density correlation to obtain the phase diagram. Dependence of biexciton properties on the electron-hole mass ratio is also discussed and the deviation from the conventional biexciton picture is clarified. In Sec. IV, the optical response of the biexciton is investigated in terms of the two-photon absorption process. Conclusions are given in Sec. V.

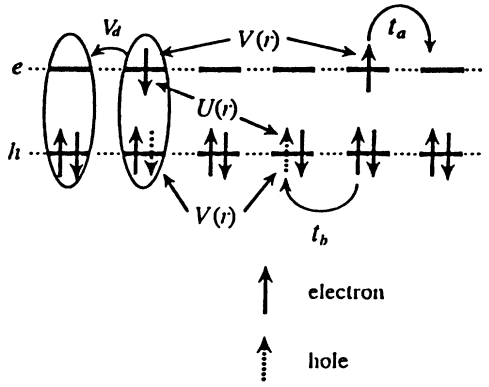

FIG. 1. The model employed in the present study.

II. THE LATTICE MODEL OF BIEXCITON

A. Hamiltonian with long-range and on-site interactions

We employ the model with long-range interactions (electron-electron and hole-hole repulsion and the electron-hole attraction) on top of the on-site interaction (the interaction within a unit cell), as depicted in Fig. 1. We consider two electron-hole pairs (two electrons in the conduction band and two holes in the valence band), where each pair is assumed to be a spin singlet, since we consider photoexcited pairs. We further assume that the two holes have antiparallel spins, since otherwise the bound states of the four fermions are not formed, due to Pauli's principle. Hence, if we neglect the electron-lattice coupling, the model Hamiltonian is expressed as[9]

$$\begin{aligned}\mathcal{H} = &-t_e \sum_{i,\sigma}(a^\dagger_{i+1,\sigma}a_{i\sigma} + \text{H.c.}) - t_h \sum_{i,\sigma}(c^\dagger_{i+1,\sigma}c_{i\sigma} + \text{H.c.}) + \varepsilon_0 \sum_{i,\sigma} c^\dagger_{i\sigma}c_{i\sigma} \\ &- \sum_{i,j,\sigma,\sigma'} U_{ij}\, a^\dagger_{i\sigma}a_{i\sigma}c^\dagger_{j\sigma'}c_{j\sigma'} + \sum_{i,j,\sigma,\sigma'} V_{ij}\left(a^\dagger_{i\sigma}a_{i\sigma}a^\dagger_{j\sigma'}a_{j\sigma'} + c^\dagger_{i\sigma}c_{i\sigma}c^\dagger_{j\sigma'}c_{i\sigma'}\right) \\ &- V_d \sum_{i,\sigma}\left(a^\dagger_{i+1,\sigma}c^\dagger_{i+1,-\sigma}c_{i,-\sigma}a_{i\sigma} + \text{H.c.}\right), \end{aligned} \tag{1}$$

where $a^\dagger_{i\sigma}$ ($c^\dagger_{i\sigma}$) creates an electron in the conduction band (a hole in the valence band) with spin σ at site i, t_e (t_h) is the transfer energy of electrons (holes), and ε_0 is the energy difference between the two orbitals from which conduction and valence bands arise. We assume the same sign for t_e and t_h (as appropriate to a semiconductor with a direct gap at Γ). The attractive electron-hole interaction between the sites i and j is denoted by U_{ij}, while V_{ij} represents the repulsive electron-electron and hole-hole interactions.

At large distances U_{ij} should behave like $1/|i-j|$, since the screening effect is negligible for a system with few electron-hole pairs. To take care of the localized nature of Wannier functions, we have in addition considered the intra-atomic energy when an electron and a hole come to the same unit cell, which we denote by $U_{ii} \equiv U_0$ and $V_{ii} \equiv V_0$. Thus, we end up with

$$U_{ij} = \begin{cases} U_0 & (i=j) \\ U_1/|i-j| & (i \neq j), \end{cases} \tag{2}$$

$$V_{ij} = \begin{cases} V_0 & (i=j) \\ V_1/|i-j| & (i \neq j), \end{cases} \tag{3}$$

where physically $U_0 > U_1 \geq 0, V_0 > V_1 \geq 0$, and we assume $V_1 = U_1$ for simplicity. Since the intraband interactions should be stronger than the interband ones,

we have $V_0 \geq U_0$. U_0, defined as the energy required to put two carriers in the same unit cell, is naturally finite. This is in sharp contrast to the continuum models, in which we have to take care of the $1/r$ singularity by such tricks as a finite cutoff in the interaction.[7,8] Hereafter the lattice constant is chosen to be the unit of length and we set $\hbar = 1$. We also take $U_0 = 1$ as a unit of energy below.

The last term in Eq. (1) represents the transfer of an electron-hole pair from site to site, which comes from the electromagnetic dipole-dipole coupling between atoms, and the value of V_d is determined by a corresponding Coulomb integral. Thus V_d, which induces a center-of-mass motion of the exciton, increases the bandwidth of the exciton:[10] an exciton becomes immobile in the Frenkel limit when we neglect this term.

In fact, the effect of V_d on the biexciton formation is of distinct interest. For a single-exciton, an introduction of V_d increases the exciton bandwidth[10] but makes the wave function for the relative motion of electron and hole more compact.[11] The former effect will favor the formation of a biexciton, while the latter will be unfavorable. Thus, we must look into these competitive effects of V_d in the formation of a biexciton. This is another strong reason why we have to treat the four-fermion problem on a lattice rather than on a continuum.

B. Numerical diagonalization

For a single exciton in a finite 1D system of length N, the Hamiltonian is expressed as a matrix of dimension N. In this case, we employ Householder's method for the diagonalization. We have checked that the size of the system is large enough by expanding the sample size until physical properties become size independent. The rate of convergence depends on the value of the parameters: larger sample sizes are required for weakly coupled excitons. For instance, while $N \leq 100$ suffices for $(t_e + t_h)/U_0 = 0.1$, $N \sim 500$ is required to make all the physical properties converge for a larger $(t_e+t_h)/U_0 = 2$.

For two electrons and two holes, the dimension of the Hamiltonian matrix becomes N^3. We take the system size of $N = 81$ ($N^3 \simeq 5.3 \times 10^5$) with periodic boundary conditions, and diagonalize the Hamiltonian (1) with the Lanczos method. The system size is large enough to attain a convergence of the physical properties when the electron-hole coupling is strong enough [$(t_e+t_h)/U_0 < 1$]. Even in a weaker-coupling case [$(t_e + t_h)/U_0 \sim 0.5$], the size of a biexciton remains of the order of ten lattice constants (see Sec. IV), so that $N = 81$ is large enough for accurate eigenvalues. On the other hand, the correlation functions, which reflect tails of the wave functions, requires N much larger than the size of an exciton, so that the correlation functions may contain some finite-size effect.

In accordance with the terminology for the strongly correlated electron systems, such as the Hubbard model in the literature, we shall use the exact diagonalization of finite systems as exact results to distinguish from approximation schemes, such as the Heitler-London approximation described later.

For finite systems, the long-range Coulomb interaction must be treated with care. A way to apply the periodic boundary condition would be to count the Coulomb interaction between particles multiply, i.e., to include the interaction with the mirror images. This would mimic a finite concentration of excitons, and is somewhat different from the weakly excited electron and hole system. To concentrate on the two-exciton problem, here we introduce a cutoff in the interaction range at half the system size. This is allowed because we are interested in bound states of excitons and the system size considered is considerably larger than the spatial extension of the bound states.

III. PROPERTIES OF SINGLE-EXCITON STATES

Before presenting the biexciton problem, we recapitulate the properties of one-exciton states in the present model.[5,11] For the system with one electron and one hole only, the repulsion between the like particles, V_{ij}, is irrelevant. Since we consider only a spin-singlet electron-hole pair created by photoexcitation, we can omit the spin indices also.

A. Excitons with finite-range interactions

If we truncate, for heuristic purposes, the interaction U_{ij} at a finite range r_c, the single-exciton problem allows algebraic solutions. The number of bound states is at most $(2r_c+1)$. For the nearest-neighbor interaction ($r_c = 1$), the lowest bound state is expressed as[5]

$$|\Psi_1^{\rm nn}\rangle = \left(\sum_i a_i^\dagger c_i^\dagger + C \sum_{i \neq j} \kappa^{|i-j|} a_i^\dagger c_j^\dagger \right) |0\rangle, \tag{4}$$

where κ is the largest positive solution of the cubic equation,

$$xy\kappa^3 + (x^2 - y)\kappa^2 + (x + xy)\kappa - x^2 = 0, \tag{5}$$

with $x \equiv t/(U_0+2V_d)$, $y \equiv U_1/(U_0+2V_d)$, and $C = t/(t-U_1\kappa)$. Here, $t \equiv t_e + t_h$, which is inversely proportional to the reduced mass of an exciton. The binding energy, E_1, is given by

$$E_1 = -t(\kappa + 1/\kappa). \tag{6}$$

The first excited exciton state is given by[11]

$$|\Psi_2^{\rm nn}\rangle = \sum_{i \neq j} \lambda^{|i-j|} (a_i^\dagger c_j^\dagger - a_j^\dagger c_i^\dagger)|0\rangle, \tag{7}$$

which exists when $\lambda \equiv t/U_1 < 1$, with an energy

$$E_2 = -t(\lambda + 1/\lambda). \tag{8}$$

The second excited state exists when

$$\frac{U_1}{U_0} > \frac{t}{U_0 - t} > 0. \tag{9}$$

The wave function and the energy have the same form as Eqs. (4)–(6) if κ is taken to be the second largest positive solution of Eq. (5). C becomes negative in this case, which makes the relative motion of the electron and hole possess two nodes as it should.

When we further simplify the model into on-site interactions only, the wave function and energy of the ground state reduce to

$$|\Phi^{\text{on-site}}\rangle = \sum_{ij} \xi^{|i-j|} a_i^\dagger c_i^\dagger |0\rangle, \tag{10}$$

$$E_1^{\text{on-site}} = -[(U_0 + 2V_d)^2 + 4t^2]^{1/2}, \tag{11}$$

with

$$\xi = \frac{[(U_0 + 2V_d)^2 + 4t^2]^{1/2} - U_0 - 2V_d}{2t}. \tag{12}$$

This is the simplification adopted by Egri,[12] whose results obtained by an approximate method coincide, somewhat accidentally, with the exact solution above.

In the one-exciton problem, $U_0 + 2V_d \cos k$ becomes a relevant energy scale, where k is the momentum of the center of mass of the electron and hole.[13] This is confirmed from the fact that $E(k) \to -(U_0 + 2V_d \cos k)$ in the Frenkel limit ($t/U_0 \to 0$). Thus, the presence of V_d effectively increases U_0 in the single-exciton problem, which also applies to the $k = 0$ states that are relevant to optical processes.

B. Wave function

The relative motion of electron and hole is described by the electron-hole density-density correlation function,

$$\alpha(r) \equiv \left\langle \sum_i \rho_{i+r}^e \rho_i^h \right\rangle_{\text{ex}} \equiv \left\langle \Psi \left| \sum_i a_{i+r}^\dagger a_{i+r} c_i^\dagger c_i \right| \Psi \right\rangle, \tag{13}$$

where $\langle\,\rangle_{\text{ex}}$ denotes the expectation value for $|\Psi\rangle$, the single-exciton wave function including both translational and relative motions. Figure 2 shows a typical exact result for the relative motion of electron and hole for the long-range Coulomb interactions ($U_0 = 2$). Each wave function exhibits an exponential decay at large distances. In the case of the on-site model ($U_1 = 0$), $\alpha(r)$ is given as

$$\alpha^{\text{on-site}}(r) = \left(\frac{1 - \xi^2}{1 + \xi^2}\right) \xi^{-2r}. \tag{14}$$

C. Binding energy

We define the binding energy of an exciton by

$$\begin{aligned} E_B(U_0, U_1, t) &\equiv -[E(U_0, U_1, t) - E(0, 0, t)] \\ &= -E(U_0, U_1, t) - 2t, \end{aligned} \tag{15}$$

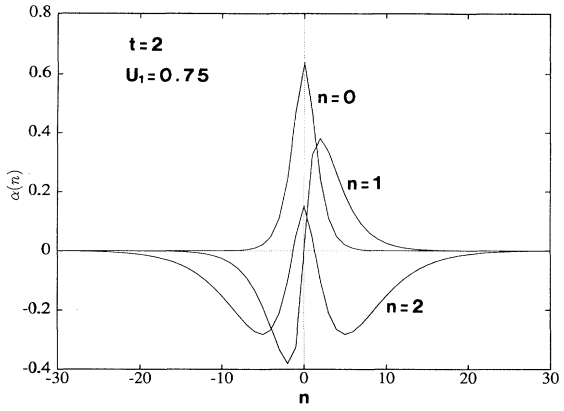

FIG. 2. Wave functions for the relative motion of the electron and hole, $\alpha(n)$, for the lowest three states are shown for $t = 1$, and $U_1 = 0.75$.

which is the energy gained by turning the interaction on. Figure 3 shows the exact result for E_B against t. It is seen that E_B decreases, but remains finite as the transfer energy is increased. This property is shared by the model with $U_1 = 0$,[11,14] for which we have

$$E_B(U_0, 0, t) = [(U_0 + 2V_d)^2 + 4t^2]^{1/2} - 2t. \tag{16}$$

Thus, an electron-hole pair is bound in 1D no matter how small the interaction between the electron and the hole may be, which is in contrast to higher-dimensional cases, where bound states only appear above some threshold strength of the interaction.

D. Frenkel exciton versus Wannier exciton

A closer look at wave functions reveals a conspicuous difference between weak-coupling and strong-coupling excitons. There is actually a *continuous* crossover between them over the whole parameter region,[5] while the usual practice is to only mention the physical property

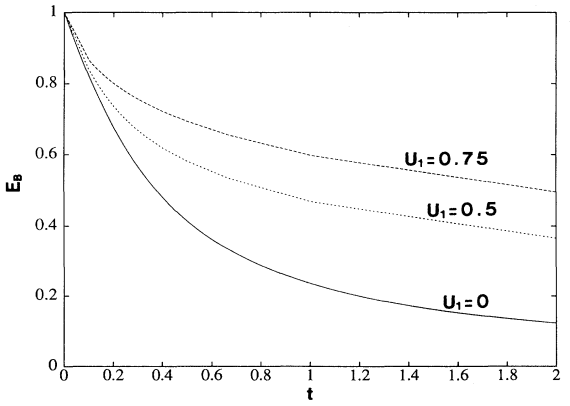

FIG. 3. The binding energy of an exciton, as a function of t for $U_1 = 0$, $U_1 = 0.5$, and $U_1 = 0.75$.

of the Wannier (strong-coupling) limit or Frenkel (weak-coupling) limit.[12]

For that we can look at the radius of the exciton, R, defined by

$$R \equiv \left\langle \sum_{ij} (i-j)^2 \rho_i^e \rho_j^h \right\rangle_{\rm ex}^{\frac{1}{2}} \tag{17}$$

as a function of t in Fig. 4, its U_1 dependence reverses as t is varied: For $t < 1$, an exciton expands with U_1, while an exciton shrinks with U_1 for $t > 1$. Interestingly, the curves for various values of U_1 cross each other near, but not exactly at, a single point. In a previous paper,[5] we have thus proposed that the change in the behavior of R may be used to define the boundary between the Frenkel and Wannier exciton regimes.

E. Bandwidth of an exciton

As mentioned in Sec. II A, V_d determines the effective mass (bandwidth) of an exciton.[10,15] We have calculated the band dispersions for the exciton for a finite $V_d = t_e/2$, with $t_e(= t_h \equiv t) = 0.1$(a), 1(b) with a fixed $U_1 = 0.75$ in Fig. 5.

The width of the lowest exciton band always increases with V_d, but its effect is more pronounced for the Frenkel exciton, in which the electron and hole are bound too tightly to move separately. The mobility of an exciton is thus primarily dominated by V_d rather than by t. In the strong-coupling limit, $t/U \to 0$, t_e and t_h, in fact, become irrelevant to the exciton bandwidth. Conversely, the electron and hole are loosely bound in a Wannier exciton, so that, in the weak-coupling limit $t/U \to \infty$, t_e and t_h dominate the exciton bandwidth and V_d exerts little effect, since the probability of finding an electron-hole pair on the same site is negligible. This is why V_d may be neglected in special cases (the Wannier limit or continuum models). We should note that V_d does not affect the bandwidth of the odd-parity excited states for which $\alpha(0) = 0$.

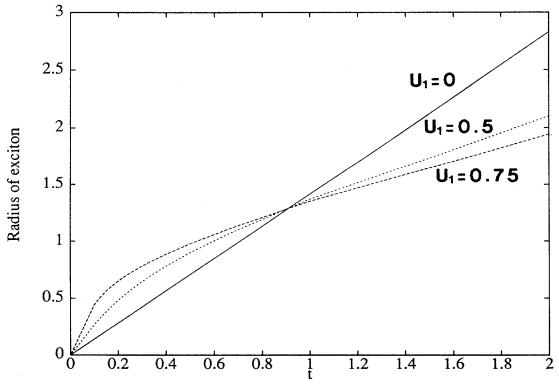

FIG. 4. The radius of the exciton, R, as a function of t for $U_1 = 0$, $U_1 = 0.5$, and $U_1 = 0.75$.

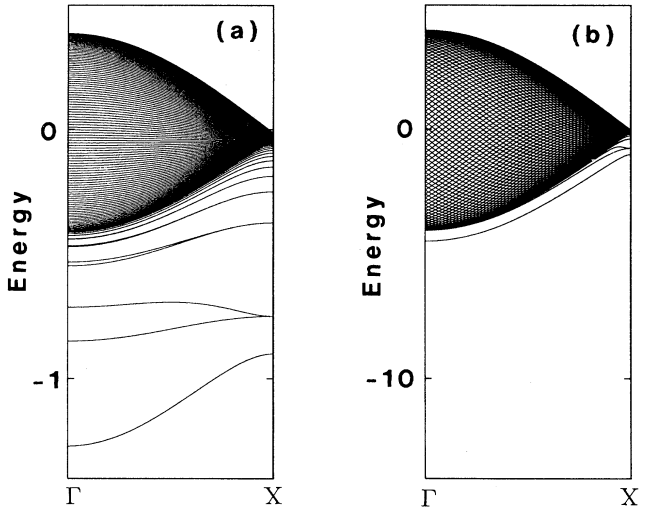

FIG. 5. The band structure of exciton for vanishing $V_d = 0$ is shown for $t_e(= t_h) = 0.1$(a), 1(b) with a fixed $U_1 = 0.75$.

Another factor that determines the bandwidth is the ratio of the effective masses between electron and hole, $\sigma \equiv m_e^*/m_h^* = t_h/t_e$. Here, we can consider $0 \le \sigma \le 1$ without a loss of generality. The width of the lowest exciton band is plotted as a function of σ for $t = 2$, $V_d = 0$, and $U_1 = 0.4$ or 0.75 in Fig. 6.

From an analogy with a hydrogen atom, $W_{\rm ex} \sim M$, decreases as σ is decreased from unity, since the total mass, $M \propto 1/t_e + 1/t_h \sim (1+\sigma)^2/\sigma$, is a decreasing function of σ. If we turn on U_0, $W_{\rm ex}$ is expressed as

$$\begin{aligned} W_{\rm ex}(U_1 = 0) &= \sqrt{1 + 4(t_e + t_h)^2} - \sqrt{1 + 4(t_e - t_h)^2} \\ &= \sqrt{1 + 4t^2} \\ &\quad - \sqrt{1 + 4t^2[(1-\sigma)/(1+\sigma)]^2}. \end{aligned} \tag{18}$$

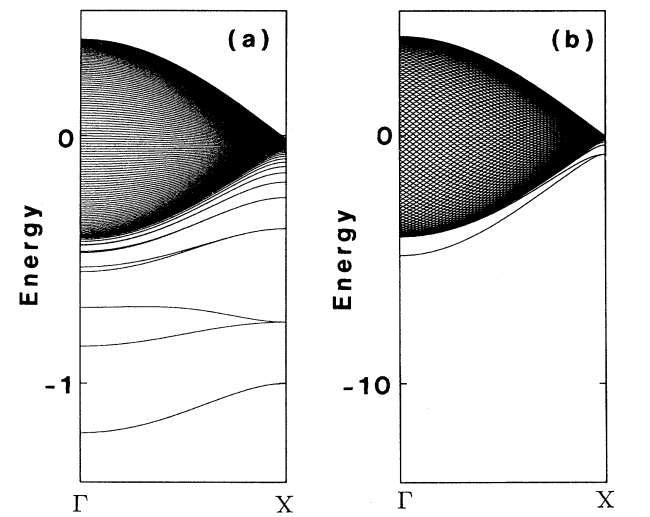

FIG. 6. The band structure of the exciton for a finite $V_d = t_e/2$ is shown for $t_e(= t_h) = 0.1$ (a), 1 (b) with a fixed $U_1 = 0.75$.

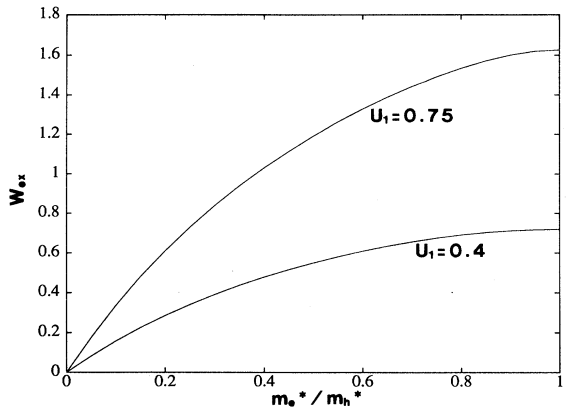

FIG. 7. The width of the lowest exciton band, as a function of $\sigma \equiv m_e^*/m_h^*$ for $t = 2$, $V_d = 0$, and $U_1 = 0.4$ and 0.75.

For a finite U_1, we have numerically calculated $W_{\rm ex}$ in Fig. 7, which is seen to again increase with σ.

As for the dependence on the interaction, $W_{\rm ex}$ increases with U_1. Namely, although the dispersion of an exciton shifts downwards with U_1, both at Γ and X points in the Brillouin zone, the shift of the former overcomes that of the latter. For the long-range Coulomb interaction (and also for finite-range ones), $W_{\rm ex}$ is given by

$$W_{\rm ex} = E(U_0, U_1, t_e - t_h) - E(U_0, U_1, t) = \frac{1-\sigma}{1+\sigma} E\left(\frac{1+\sigma}{1-\sigma}U_0, \frac{1+\sigma}{1-\sigma}U_1, t\right) - E(U_0, U_1, t). \tag{19}$$

Since $E(\infty, U_1, t)(\to -U_0)$ is finite, the first term becomes negligible in the vicinity of $\sigma = 1$. Hence the decrease of the second term causes an increase in $W_{\rm ex}$.

IV. PROPERTIES OF BIEXCITON STATES

We now come to our original question of the formation of a biexciton. To discriminate a biexciton from two unbound excitons, we have looked into two quantities.

(a) Binding energy of a biexciton — This is defined as the energy required to separate two excitons to an infinite distance,

$$E_{\rm biex} \equiv -(E_{2e2h} - 2E_B), \tag{20}$$

where E_B is the energy of a single exciton calculated in Sec. III (Ref. 5) and E_{2e2h} is the energy of the four-fermion system. A positive $E_{\rm biex}$ implies that a biexciton is formed, while a negative $E_{\rm biex}$ means that two excitons repel each other. In this case, a finite $|E_{\rm biex}|$ is an artifact of confining them to a finite system: the quantity will vanish in the thermodynamic limit.

(b) Hole-hole correlation function — the spatial extension of the biexciton is usually evaluated from the hole-hole correlation function,[8] which, in the Heitler-London approximation, reduces to the wave function for the relative motion, i.e., the biexciton wave function. The function is defined as

$$\zeta^{\rm hh}(r) = \left\langle \sum_i c^\dagger_{i+r\uparrow} c_{i+r\uparrow} c^\dagger_{i\downarrow} c_{i\downarrow} \right\rangle_{\rm biex}, \tag{21}$$

where $\langle\ \rangle_{\rm biex}$ is the expectation value for the biexciton wave function. From this quantity, we can identify whether the two like particles, despite their repulsion, participate in the bound state, due to the presence of the carriers of opposite charge in analogy with a hydrogen molecule.

We first discuss the case with $V_d = 0$, while the effect of V_d will be discussed in the last subsection.

A. Biexciton binding energy

1. Weak- and strong-coupling regimes

Figure 8 shows $E_{\rm biex}$ as a function of $t \equiv t_e + t_h$ for $U_1 = 0$ or 0.75 with $V_0 = U_0$ and $m_e^*/m_h^* = 1$. $E_{\rm biex}$ increases with t for both on-site interactions and long-range interactions with each curve starting from $E_{\rm biex} = 0$ at $t = 0$, which is obvious from the static configurations of electrons and holes. The result, which shows that $E_{\rm biex}$ is an increasing function of t/U_0 for $t < 2$, is in contrast with the prediction of the continuum models, which show that the binding energy of a biexciton is a decreasing function of the strength of Coulomb interaction.[16] We identify this as an indication that continuum models fail to describe the atomic-scale behavior of the biexciton wave function. However, $E_{\rm biex}$ should eventually decrease to zero as t goes to infinity, since the results in the weak-coupling regime should coincide with those with continuum models.

When the strength of the Coulomb repulsion V_0 between like particles is increased, the formation of a biexciton becomes less favorable. Figure 9 for $E_{\rm biex}$ as a function of the ratio, V_0/U_0, indeed shows that $E_{\rm biex}$ monotonically decreases as V_0/U_0 is increased from unity.

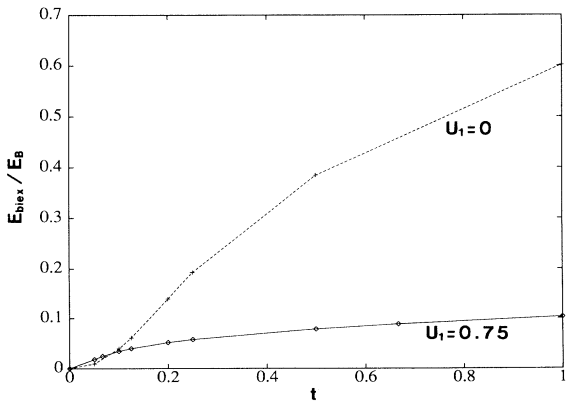

FIG. 8. The binding energy of a biexciton for $m_e^*/m_h^* = 1$, as a function of t for $U_1 = 0$ and $U_1 = 0.75$, with a fixed $V_0/U_0 = 1$ and $V_d = 0$.

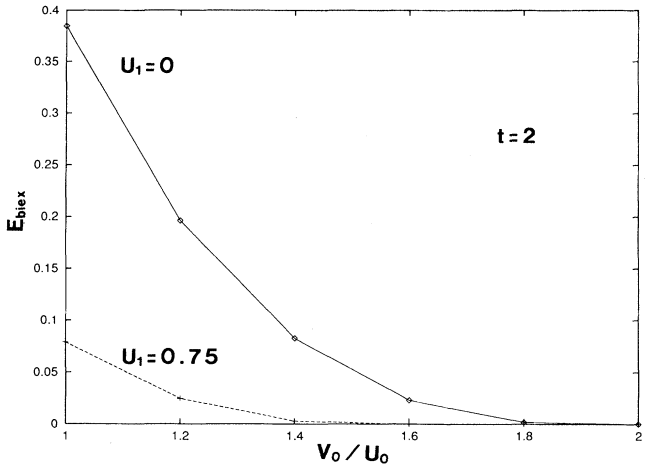

FIG. 9. The binding energy of a biexciton for $m_e^*/m_h^* = 1$, as a function of V_0/U_0 for $U_1 = 0$ and $U_1 = 0.75$, with a fixed transfer $t = 1$ and $V_d = 0$.

However, the binding energy does not vanish even when V_0/U_0 is as large as 1.5. There the exciton wave function (relative motion) spreads over several lattice spacings for $t = 2$, and this will "dilute" the effect of V_0 to favor the formation of a biexciton.

2. Dependence on U_1/U_0

While continuum models in the existing literature concern long-range interactions only, here, we can single out the effect of the strength of the long-range interaction, U_1, *relative to* the on-site interaction ($U_0 = 1$) in the formation of a biexciton. The result for $E_{\rm biex}$ as a function of U_1 (Fig. 10) shows that the effect of U_1 *reverses* as we vary the value of U_0: When the coupling is weak, $t/U_0 > 0.1$, $E_{\rm biex}$ increases with U_1, while $E_{\rm biex}$ decreases with U_1 for a strong coupling, $t/U_0 < 0.1$. This crossover may be understood in terms of the single-exciton states, which is discussed in Sec. IV D on the phase diagram.

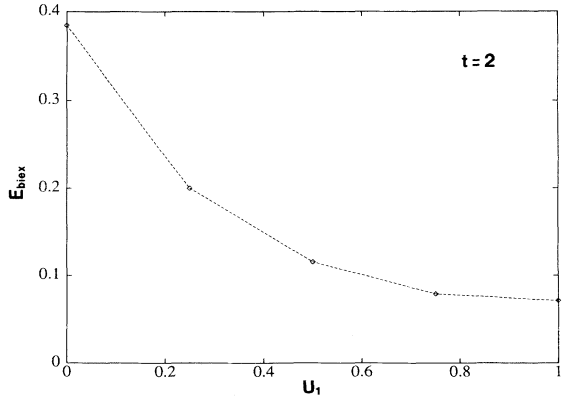

FIG. 10. The binding energy of a biexciton for $m_e^*/m_h^* = 1$, as a function of U_1, with $V_0/U_0 = 1$ and $t = 2$.

3. Mass ratio

The dependence of $E_{\rm biex}$ on the mass ratio, $\sigma \equiv m_e^*/m_h^*$, has been investigated by various authors for 2D systems[17] and 3D systems,[1,2,18] as well as for 1D systems.[8] For the present model, we show in Fig. 11 the exact result for $E_{\rm biex}$ normalized by E_B (the binding energy of a single exciton), as a function of $\sigma = t_h/t_e = m_e^*/m_h^*$.

We first note that the absolute value, $|E_{\rm biex}/E_B|$, monotonically increases as a function of σ. This is understood in a manner similar to that provided by Wehner[19] and by Adamowski *et al.*[20] for continuum models. We can also prove that the derivative, $d(E_{\rm biex}/E_B)/d\sigma$, vanishes at $\sigma = 1$.

As the transfer energy t decreases, $d(E_{\rm biex}/E_B)/d\sigma$ for a fixed σ becomes smaller. Since the bandwidth of a single exciton increases with σ as shown in the last section, the loss in the kinetic energy in forming a biexciton becomes larger for larger σ. Thus, $E_{\rm biex}/E_B$ decreases with σ. On the other hand, the derivative of the bandwidth of an exciton, $dW_{\rm ex}/d\sigma$, is smaller for the strong-coupling case (see Fig. 7). Hence, $E_{\rm biex}/E_B$ varies less pronouncedly with σ for a stronger electron-hole coupling.

B. Correlation functions: Comparison with the Heitler-London approach

1. Heitler-London approximation

Now we turn to the validity of the variational and Heitler-London approaches for the biexciton, which is one of the key questions raised in the Introduction. Since a Heitler-London approximation disregards the four-fermion correlation effect, we can see to what extent the correlation is appreciable.

The Heitler-London approximation may be applied to the present model in the following manner. First, we

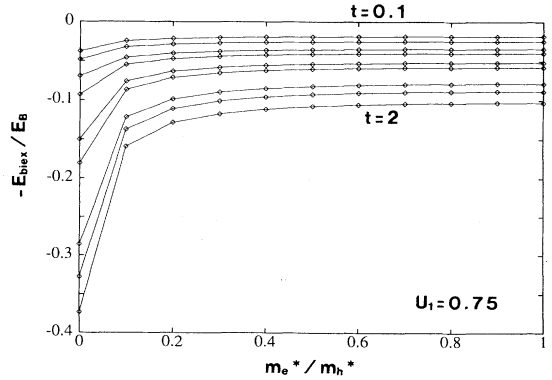

FIG. 11. The binding energy of a biexciton, as a function of the mass ratio, $\sigma \equiv m_e^*/m_h^*$, for $t = 0.1$, 0.15, 0.2, 0.25, 0.4, 0.5, 1, 1.33, and 2, from top to bottom with $U_1 = 0.75$ and $V_d = 0$.

introduce a trial wave function $|\Psi_{\rm HL}\rangle$ defined by

$$|\Psi_{\rm HL}\rangle = \sum_{ijkl} f(i,j)(\langle i\uparrow; k\downarrow|\phi\rangle\langle j\downarrow; l\uparrow|\phi\rangle|ij;kl\rangle - \langle i\uparrow; l\downarrow|\phi\rangle\langle j\downarrow; k\uparrow|\phi\rangle|ij;lk\rangle), = \sum_{ijkl} f(i,j)\hat{\phi}(i,j;k,l)|ij;kl\rangle, \quad (22)$$

where

$$|ij;kl\rangle = a^\dagger_{i\uparrow}a^\dagger_{j\downarrow}c^\dagger_{k\uparrow}c^\dagger_{l\downarrow}|0\rangle \quad (23)$$

and

$$|i\sigma;j\sigma'\rangle = a^\dagger_{i\sigma}c^\dagger_{j\sigma'}|0\rangle. \quad (24)$$

$|\phi\rangle$ denotes the lowest single exciton, and $f(i,j)$ is the biexciton wave function usually discussed in former studies and corresponds to $\zeta^{\rm hh}(r)$ in the present paper. We have then numerically solved the secular equation determining $f(i,j)$,

$$\sum_{i'j'}\sum_{klk'l'} \hat{\phi}^*(i,j;k,l)\langle ij;kl|\mathcal{H}|i'j';k'l'\rangle \times\hat{\phi}(i',j';k',l')f(i',j') = Ef(i,j), \quad (25)$$

to obtain Heitler-London results for the present model. Figure 12 shows that $E_{\rm biex}$ in the Heitler-London scheme gives only about half the exact result for the whole range of t. This discrepancy indicates that the correlation effect is, in fact, significant, and the Heitler-London approximation is inadequate.

2. *Electron-hole density correlation*

To elaborate how these approximations fail, we have calculated, in addition to the hole-hole correlation, the electron-hole density correlation function defined by

$$\zeta^{\rm eh}_{\sigma\sigma'}(r) \equiv \left\langle \sum_i a^\dagger_{i\sigma}a_{i\sigma}c^\dagger_{i+r,\sigma'}c_{i+r,\sigma'} \right\rangle_{\rm biex}. \quad (26)$$

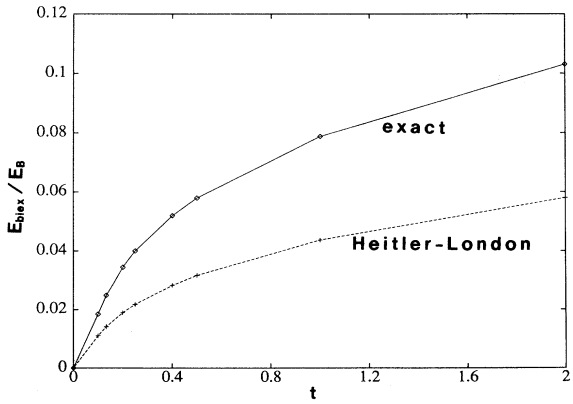

FIG. 12. The exact result and the Heitler-London result for the binding energy of a biexciton, $E_{\rm biex}$, as a function of t for $U_1 = 0.75$, $V_d = 0$, and $V_0/U_0 = 1$.

A typical result for $\zeta^{\rm eh}_{\uparrow\downarrow}(r)$ is given in Fig. 13. The figure covers both the biexciton regime ($V_0/U_0 = 1$) and the unbound regime ($V_0/U_0 = 1.5$), and the decay of $\zeta^{\rm eh}_{\uparrow\downarrow}$ is seen to be faster when the electrons and holes are bound into a biexciton. When the biexciton is formed, $\zeta^{\rm eh}_{\uparrow\downarrow}(r)$ for the biexciton system, which cannot be fitted to a single exponential form, deviates at large distances from that for a single exciton, $\zeta^{\rm eh}_{\uparrow\downarrow}$ (single-exciton) $\sim \exp(-3.36r)$.[5] As for the spin indices, $\zeta^{\rm eh}_{\sigma\sigma}(r) \neq \zeta^{\rm eh}_{\sigma,-\sigma}(r)$ only when $V_d \neq 0$, which is discussed later.

When we apply the Heitler-London approximation to the present model, we find that the hole-hole correlation, $\zeta^{\rm hh}(r)$, is more spatially extended as shown in Fig. 14. Even when we turn to a variational approach, which could potentially go beyond the Heitler-London approximation, there remains the problem of how to choose trial functions for the biexciton state. Already for the single-exciton state, there exist no analytical wave functions when we consider long-range interactions ($U_1 \neq 0$), which play an important role in the biexciton formation. In the weak-coupling limit, however, the electron-hole (relative) motion asymptotically becomes exponential.

Hence, the approximations compared here are expected to give reasonable results only when the electron-hole relative motion is spatially extended. Wannier excitons in higher dimensions correspond to this case. We stress, however, that in 1D systems the correlated motion of electrons and holes over the length scale of lattice constant as exhibited in a structure in $\zeta^{\rm eh}_{\sigma\sigma'}(r)$ is essential even in the weak-coupling case, which is why the approximations become unreliable.

C. Correlation functions: comparison with continuum models

We now turn to a comparison with continuum models for the correlation functions. Bányai *et al.*[8] have calculated the wave function of the relative motion of two holes

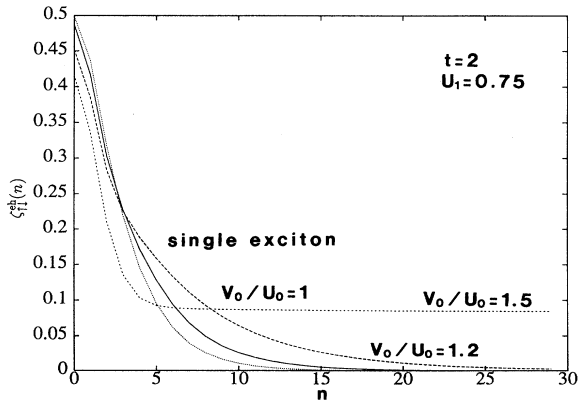

FIG. 13. The electron-hole density correlation function, $\zeta^{\rm eh}_{\uparrow\downarrow}(r)$, for $m^*_e/m^*_h = 1$ for $V_0/U_0 = 1$, $V_0/U_0 = 1.2$, and $V_0/U_0 = 1.5$ with fixed $t = 2$, $V_d = 0$, and $U_1 = 0.75$. The line denoted as "single" shows the correlation function for a single exciton.

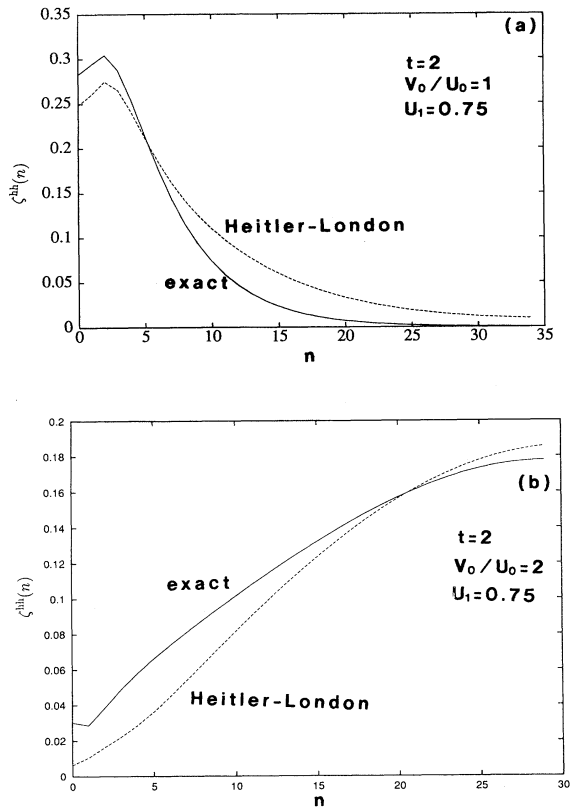

FIG. 14. The hole-hole correlation function, $\zeta^{\rm hh}(r)$, for $V_0/U_0 = 1$ (a) or 2 (b) with fixed $t = 2$, $U_1 = 0.75$, $V_d = 0$ and $m_e^*/m_h^* = 1$. The correlation function calculated with Heitler-London approximation is shown in each figure.

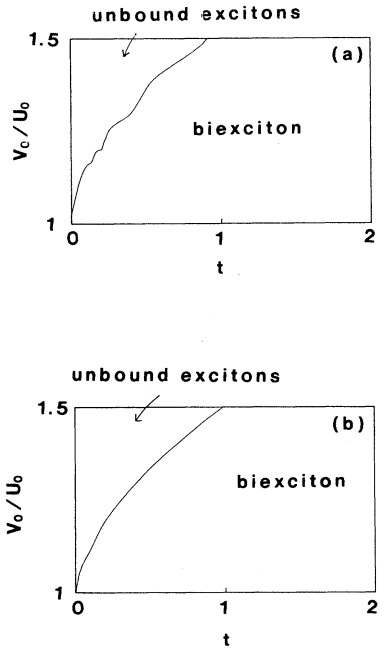

FIG. 15. Phase diagram on the $(t, U_0/V_0)$ plane for the biexciton state for (a) $U_1 = 0$ and (b) $U_1 = 0.75$ with $m_e^*/m_h^* = 1$ and $V_d = 0$.

in a continuum model within an approximation that separates the four-fermion wave function into an electron-hole part and a hole-hole part. As an electron-hole wave function, they have assumed a product of the single-exciton wave function, thereby neglecting its deformation due to the many-body effect. Although their result reproduces a known tendency that the biexciton binding energy is larger for lower dimensions,[1,17] the quantitative accuracy of their approximation is not clear, especially for 1D biexcitons.

Here, we present a numerical result for the correlation functions to explore this point. For the typical cases of (a) a biexciton and (b) unbound excitons, the hole-hole correlation function $\zeta^{\rm hh}(r)$ [Eq. (21)] is shown in Fig. 14. The result implies that Banyai's approximation holds only in the weak-coupling regime, where the hole-hole correlation is peaked at a finite distance [Fig. 14(a)], while $\zeta^{\rm hh}(r)$ decays faster for the strong-coupling regime, where a biexciton is more compact and the size of the biexciton is of an *atomic* scale.

D. Phase diagram for $V_d = 0$

Now we discuss the phase diagram (Fig. 15) for the biexciton system on the plane of the transfer ($t \equiv t_e + t_h$) and the ratio ($V_0/U_0 \geq 1$) of the electron-electron repulsion and the electron-hole attraction with $m_e^*/m_h^* = 1$ and $V_d = 0$. The figure depicts the contour representing $E_{\rm biex} = 0$, which gives the boundary between the biexciton regime and the unbound regime. The boundary should start from the point $t = 0$, $V_0/U_0 = 1$, since a biexciton is formed for $U > V$, while it decomposes for $U < V$ when $t = 0$.

If we compare the result for $U_1 = 0$ [Fig. 15(a)] and $U_1 = 0.75$ [Fig. 15(b)], the long-range interaction is seen to play a critical role in the formation of biexcitons. Namely, whereas long-range interactions exert an *unfavorable* effect on the biexciton formation in the weak-coupling regime, the formation of biexciton is *favored* by the presence of long-range interactions in the strong-coupling regime. These opposite tendencies make the two lines in (a) and (b) cross, where the crossover occurs around $t \sim 0.1$.

If we recall the behavior of the radius, R, of a single exciton as a function of t and U_1 presented in Sec. III, the introduction of the long-range interaction increases R in the strong-coupling (Frenkel) regime, while it decreases R in the weak-coupling (Wannier) regime. If we fit this result to the effect of the long-range interaction favoring (suppressing) the formation of biexcitons in the Frenkel (Wannier) regime, we may postulate that the formation of a biexciton is favored as the spatial extension of the relative motion of an electron and a hole increases. Thus, an important finding here is that the Frenkel-Wannier crossover does appear in the biexciton phase diagram as well.

E. Effect of dipole-dipole interactions

As we have stressed in Sec. III D V_d affects both the relative and translational motions of single excitons. Now the problem is the effect of V_d on biexciton formation, which is only relevant to singlet electron-hole pairs as seen from the Hamiltonian, Eq. (1).

To detect the effect of V_d, we show in Fig. 16 a typical result for the hole-hole density correlation function, $\zeta^{\rm hh}(r)$, along with the electron-hole density correlation function [Eq. (26)] in the biexciton state. By looking at the latter, we can see how each exciton is deformed in a biexciton, or how the Heitler-London picture modifies into a "molecular orbital" picture. The wave function of one-exciton state for the same values of parameters is also displayed in the figure for comparison. It is seen that $\zeta^{\rm eh}_{\uparrow\downarrow}(r)$ does not significantly deviate from the one-exciton wave function, while $\zeta^{\rm eh}_{\downarrow\downarrow}(r)$ almost coincides with $\zeta^{\rm hh}(r)$.

From this we can see that a finite V_d drastically changes the picture of a biexciton back into a weakly interacting two excitons having a weak "covalent bond" (in analogy with a hydrogen molecule). When each exciton is slightly deformed, the exciton-exciton interaction is weak, since it is an interaction between neutral objects. A loosely bound exciton has a $\zeta^{\rm hh}(r)$ spreading beyond the system size ($N = 81$) considered here.

For the physical case of V_0 exceeding U_0, the biexciton state becomes rapidly unstable, and a biexciton is broken into two excitons even when V_0 ($= 1.1U_0$) exceeds U_0 only slightly. Thus, the phase diagram is completely different from the $V_d = 0$ result (Fig. 15). This implies that biexcitons in realistic conditions exist only for a stringent condition of very small V_d.

V. TWO-PHOTON ABSORPTION

One way to experimentally detect biexcitons is the two-photon absorption (TPA). Within the electric-dipole approximation, the interaction between an electron-hole system and electromagnetic waves is described by the Hamiltonian,

$$\mathcal{H}_{\rm int} = -\sum_{ij\sigma}\left(D^{\rm eh}_{ij} a^\dagger_{i\sigma} c^\dagger_{j,-\sigma} + D^{\rm ee}_{ij} a^\dagger_{i\sigma} a_{j\sigma} + D^{\rm hh}_{ij} c^\dagger_{i\sigma} c_{j\sigma} \right) + \text{H.c.} \tag{27}$$

Here, the first term creates an electron-hole pair, and the second (third) term transfers an electron (hole) from site j to i. The dipole matrix element in an electric field $\mathbf{E}_0$ is defined as

$$D^{\alpha\beta}_{ij} \equiv \langle \alpha i | D | \beta j \rangle, \tag{28}$$

where we have $D = \mathbf{r}\cdot\mathbf{E}_0 \cos\omega t$ for an incident light of frequency ω, and $|\alpha i\rangle$ denotes an orbital in the conduction band ($\alpha = e$) or the valence band (h) at site i (see the Appendix).

The polarization dependence of the TPA in one-dimensional exciton systems has been discussed in Ref. 21 and we assume here that the polarization of the light is parallel to the chain. The orbitals in the valence and conduction bands in each unit cell are assumed to have different parities to allow the optical transition to the lowest exciton state. This assumption is justified for polysilane from both the experimental results for absorption spectra[22,23] and the theoretical band calculation.[24]

In the TPA process, the one-exciton states enter as intermediate states of the second-order optical process, and all the terms in Eq. (27) are relevant. The TPA transition rate is then given by

$$A_{\rm TPA}(\omega) \propto \sum_\mu \left| \sum_\nu \frac{\langle \mu | D | \nu \rangle \langle \nu | D | 0 \rangle}{\omega - E_\nu} \right|^2 \delta(2\omega - E_\mu), \tag{29}$$

where $|0\rangle$ denotes the initial state with no exciton, $|\nu\rangle$ the intermediate state, and $|\mu\rangle$ the final state with two electron-hole pairs. The quantity $A_{\rm TPA}(\omega)$ is proportional to $\mathrm{Im}\chi^{(3)}$, where $\chi^{(3)}$ is the third-order nonlinear susceptibility for the TPA process.[25] Here, we shall choose the lowest two-electron two-hole state as $|\mu\rangle$.

The numerical result for the TPA spectrum is shown in Fig. 17 for various values of t, with $U_0 = V_0$, $U_1 = 0.75$, and $V_d = 0$ for near one-photon resonance. The larger peaks come from the biexciton, while the small ones are due to the single-exciton resonance. Thus, the energy difference between these peaks gives the binding energy of a biexciton.

The biexciton peak is always larger than the single-exciton peak, since the matrix element between the lowest exciton state (as an intermediate state) and the biexciton state is enhanced, due to the deformation of the four-body wave function. This is a typical biexciton effect in TPA spectrum, which appears irrespective of the dimensionality of the system. If we turn on V_d, this drastically reduces $E_{\rm biex}$, so that it becomes difficult to distinguish two peaks in TPA spectrum for a finite V_d.

As for the t dependence, the TPA response is found

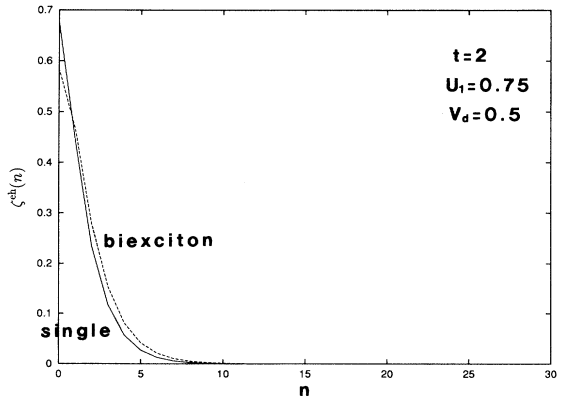

FIG. 16. The hole-hole correlation function and the electron-hole density correlation function, $\zeta^{\rm eh}_{\uparrow\downarrow}(r)$, for $m^*_e/m^*_h = 1$, $t = 2$, $V_d = 0.5$, and $U_1 = 0.75$.

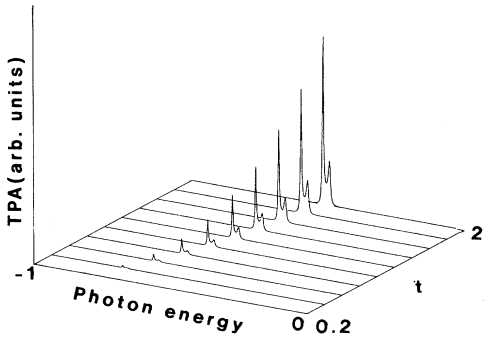

FIG. 17. Two-photon absorption spectrum near one-photon resonance is shown for various values of t with $U_1 = 0.75$, $V_d = 0$, and $V_0/U_0 = 1$.

to be more intense in the Wannier regime than in the Frenkel regime, in contrast to the one-photon absorption. If we remember that the spatial extension of the biexciton decreases as t decreases, Fig. 17 is reminiscent of the "giant oscillator strength" in the two-photon absorption known in 3D continuum models.[26] Here, however, the different behaviors in the Frenkel and Wannier regimes come not simply from the spatial extension as in the ordinary giant TPA, but also from the deformation of wave functions from a biexciton effect.

VI. CONCLUSION

We have studied the formation of a biexciton in a 1D lattice model in the coexistence of long-range Coulomb and on-site interactions. We have concluded the following.

(1) Different effects of long-range interaction on the formation of a biexciton may be used to identify Frenkel and Wannier regimes, which goes hand in hand with the crossover for single excitons.

(2) The formation of a biexciton also involves a competition between the electron-electron repulsion (V_0) and the electron-hole attraction (U_0), so that the ratio V_0/U_0 is crucial.

(3) The electromagnetic dipole-dipole coupling, which transfers the electron-hole pair, drastically affects the biexciton phase diagram.

(4) The deformation of the constituent exciton (relative motion of an electron and a hole) on atomic scales invalidates the conventional (Heitler-London, variational or continuum) models, especially when the electron and hole masses are similar ($\sigma \sim 1$).

(5) The same deformation accounts for an effect of biexciton formation on the two-photon absorption (TPA). To be more precise, the oscillator strength of the TPA is larger in the Wannier regime than in the Frenkel regime, in contrast to the one-photon absorption. The difference is a biexciton effect, which is the enhancement of polarization, due to the deformation of the relative motion of electrons and holes.

The message here is that a crucial factor in the biexciton formation is the carrier correlation (deformation of the electron-hole wave function from a simple superposition of two-exciton wave functions) *on atomic length scales.*

ACKNOWLEDGMENTS

The authors are grateful to Professor Y. Tokura for discussions on the experimental results on polysilane, and Dr. T. Chikyu for collaboration on the single-exciton problem. They also thank Professor S. Tsuneyuki and Dr. K. Shiraishi, Dr. K. Kobayashi, Dr. K. Kuroki, and Dr. S. Abe for valuable discussions. Numerical calculations were performed on HITAC S-820/80 and M-880 at the Computer Center of the University of Tokyo. This work is in part supported by a Grant-in-Aid from the Ministry of Education, Science, and Culture of Japan.

APPENDIX: MATRIX ELEMENTS OF THE DIPOLE MOMENT

The matrix element of the dipole moment may be calculated by taking the Slater orbital as the radial part of the atomic orbital assigned to each site. As for the angular part, we take s orbitals for the atomic orbitals that constitute the valence band and p_z orbitals (with z-axis along the chain) for the conduction band. This makes the direct transition at the band edge optically allowed. If the radial part of the Slater orbital is denoted to be $\propto \exp(-r/d)$, the matrix elements are given as

$$D_{ij}^{\mathrm{ee}} = \frac{(i-j)}{3}\left[\left(\frac{|i-j|}{d}\right)^2 + 3\frac{|i-j|}{d} + 3\right]\exp\left(-\frac{|i-j|}{d}\right),$$

$$D_{ij}^{\mathrm{hh}} = (i-j)\left[-\left(\frac{|i-j|}{d}\right)^2 + \frac{|i-j|}{d} + 1\right]\exp\left(-\frac{|i-j|}{d}\right), \tag{A1}$$

$$D_{ij}^{\mathrm{eh}} = \frac{\sqrt{3}d}{6}\left[\left(\frac{|i-j|}{d}\right)^3 + 2\left(\frac{|i-j|}{d}\right)^2 + 3\frac{|i-j|}{d} + 3\right]\exp\left(-\frac{|i-j|}{d}\right).$$

Here, d is the effective range of the dipole moment, to which the value of the matrix elements is sensitive. In the present calculation, d is set equal to 0.3 in units of the lattice constant, which is considered to be a reasonable value for polysilane.

* Present address: Advanced Research Laboratory, Toshiba Corporation, Kawasaki 210, Japan.
[1] O. Akimoto and E. Hanamura, Solid State Commun. **10**, 253 (1972).
[2] W. F. Brinkman, T. M. Rice, and B. Bell, Phys. Rev. B **8**, 1570 (1973).
[3] E. Hanamura and H. Haug, Phys. Rep. **33**, 209 (1977).
[4] N. B. An, H. N. Cam, and N. T. Dan, J. Phys. Condens. Matter **3**, 3317 (1991).
[5] K. Ishida, T. Chikyu, and H. Aoki, Phys. Rev. B **47**, 7594 (1993).
[6] T. Hasegawa, Ph.D. thesis, University of Tokyo, 1993.
[7] T. Ogawa and T. Takagahara, Phys. Rev. B **44**, 8138 (1991); Surf. Sci. **263**, 506 (1992).
[8] L. Bányai, I. Galbraith, C. Ell, and H. Haug, Phys. Rev. B **36**, 6099 (1987).
[9] K. Ishida and H. Aoki, in *Proceedings of the 21st International Conference on Physics of Semiconductors, Beijing, 1992* (World Scientific, Singapore, 1993), p. 213. The phase diagram given there is qualitatively correct.
[10] R. W. Heller and A. Marcus, Phys. Rev. **84**, 809 (1951).
[11] K. Ishida, Ph.D. thesis, University of Tokyo, 1991.
[12] I. Egri, J. Phys. C **22**, 1843 (1979).
[13] J. Frenkel, Phys. Rev. **37**, 17 (1931); **37**, 1276 (1931).
[14] T. Chikyu (unpublished).
[15] J.-P. Gallinar and D. C. Mattis, Phys. Rev. B **32**, 4914 (1985).
[16] The strength of Coulomb interaction is determined by the thickness of wire in quantum wires, since the thickness dominates the effective strength of the electron-hole interaction at short distances. See, e.g., Refs. 7 and 8.
[17] J. L. Zhu, X. Chen, and J. J. Xiong, J. Phys. Condens. Matter **3**, 9559 (1991); D. A. Kleinman, Phys. Rev. B **28**, 871 (1983); R. C. Miller, D. A. Kleinman, A. C. Gossard, and O. Munteanu, *ibid.* **25**, 6545 (1982).
[18] M. A. Lee, P. Vashishta, and R. K. Kalia, Phys. Rev. Lett. **51**, 2422 (1983); A. C. Cancio and Y.-C. Chang, Phys. Rev. B **42**, 11 317 (1990).
[19] R. K. Wehner, Solid State Commun. **7**, 457 (1969).
[20] J. Adamowski, S. Bednarek, and M. Suffczyński, Philos. Mag. **26**, 143 (1972).
[21] A. Shimizu, T. Ogawa, and H. Sakaki, Phys. Rev. B **45**, 11 338 (1992); T. Ogawa and A. Shimizu, *ibid.* **48**, 4910 (1993).
[22] H. Tachibana, Y. Kawabata, S. Koshihara, T. Arima, H. Moritomo, and Y. Tokura, Phys. Rev. B **44**, 5487 (1991).
[23] H. Tachibana *et al.*, Phys. Rev. B **45**, 8752 (1992); **47**, 4363 (1993).
[24] K. Takeda and K. Shiraishi, Phys. Rev. B **39**, 11 028 (1989).
[25] See, e.g., Y. R. Shen, *The Principles of Nonlinear Optics* (Wiley, New York, 1984).
[26] E. Hanamura, Solid State Commun. **12**, 951 (1973).